INSTITUTE OF PHYSICS PUBLISHING MEASUREMENT SCIENCE AND TECHNOLOGY
Meas. Sci. Technol. **13** (2002) 807–819 PII: S0957-0233(02)32732-2

Developing a non-intrusive measuring technique for determining orthokinetic agglomeration rate constants

E D Hollander[1,2], J J Derksen[1], H J M Kramer[2] and H E A Van den Akker[1]

[1] Kramers Laboratorium voor Fysische Technologie, Prins Bernhardlaan 6, Delft University of Technology, 2628 BW Delft, The Netherlands
[2] Laboratory for Process Equipment, Delft University of Technology, Leeghwaterstraat 44, 2628 CA Delft, The Netherlands

E-mail: j.j.derksen@tnw.tudelft.nl

Received 15 January 2002, in final form 12 March 2002, accepted for publication 22 March 2002
Published 18 April 2002
Online at stacks.iop.org/MST/13/807

Abstract
A non-intrusive technique has been developed for measuring agglomeration rate constants (β_0) in a constant shear field. A particulate suspension with a mean particle diameter, d, of about 10 μm is introduced in an optically accessible cylindrical Couette flow device. The suspension is illuminated by means of a pulsed laser and observed with a CCD camera. The recorded images are analysed off-line to determine the particle number concentration and a measure of the particle size. The time evolution of these quantities is fitted to an agglomeration rate law, from which the agglomeration rate constant is subsequently derived. By varying the rotational speed of the outer cylinder, different shear rates can be applied to the suspension. The full shear rate dependence of the agglomeration rate constant can be measured this way. Test results show that the set-up is well suited to determining particle concentrations, while only relative particle size information could be obtained. The measured signal shows a linear response to the suspension concentration and obeys the expected Poisson statistics. One set of agglomeration rate constants, measured at seven different shear rates between 15 and 55 s^{-1}, was obtained. A distinct maximum for β_0 was found at a shear rate of 30 s^{-1}, which will be the subject of further study.

Keywords: particle number concentration, particle size, Couette flow, microscopy, orthokinetic agglomeration, industrial crystallization

List of symbols

a	centrifugal acceleration (m s^{-2})
a_1, a_2	fitting parameters
c	particle concentration in frame units (frame^{-1})
d	particle diameter (m)
d_1, d_2	diameter of particle 1, 2 (m)
g	gravitational acceleration constant (m s^{-2})
k_b	Boltzmann constant (J K^{-1})
I,I_{max}	(maximum) image intensity (arb. units)
m_0	zeroth moment of the PSD (m^{-3})
m_{00}	initial zeroth moment of the PSD (m^{-3})
N_1, N_2	particle number density of size 1, 2 (m^{-3})
NA	numerical aperture
r_0, r_{12}	agglomeration rate (m^{-3} s^{-1})
r	radial coordinate (m)
R_i, R_o	inner, outer cylinder size (m)
s	Gauss filter width
S	super-saturation
t_{exp}	exposure time (s)
T	temperature (K)

v_p	particle velocity (m s^{-1})
$v_{p,r}$	radial particle velocity (m s^{-1})
v_θ	tangential velocity (m s^{-1})
x_g	pixel coordinate
β_0, β_{12}	agglomeration kernel (m^3 s^{-1})
$\dot{\gamma}$	shear rate (s^{-1})
δ	optical resolution (m)
ϵ	turbulent energy dissipation rate (m^2 s^{-3})
η	dynamic fluid viscosity (kg m^{-1} s^{-1})
λ	wavelength of light (m)
λ_k	Kolmogorov length scale (m)
μ	average particle concentration ($frame^{-1}$)
ν	kinematic fluid viscosity (m^2 s^{-1})
$\Delta\rho$	particle–liquid density difference (kg m^{-3})
ψ	collision efficiency
ω	angular velocity (rad s^{-1})
PDF	probability density function
PFR	Poiseuille flow reactor
PSD	particle size distribution
STR	stirred tank reactor

1. Introduction

Agglomeration is a secondary process frequently encountered in reactive crystallization. Particles collide, cement together due to deposition of material on the contact plane of the particles, and may continue as an agglomerate (figure 1). Due to the significant influence of this mechanism on the product quality (e.g. the particle size distribution), it is essential to incorporate this mechanism in, for example, reactor design procedures. Due to the complex interactions between hydrodynamics and agglomeration, this mechanism is often improperly accounted for, or even completely disregarded.

It has been known for decades that agglomeration in aqueous systems of particles with a size of around 10 μm is affected significantly by fluid flow. In 1917, Von Smoluchowski [1] analytically derived that the particle collision rate in a two-dimensional shear flow is proportional to the applied shear rate. Deriving the accompanying agglomeration rate is more difficult, however, due to strong non-linear interactions between hydrodynamics, chemistry and agglomeration. At increasing shear rates, the number of collisions will increase, but the particle contact time (i.e. the time the particles have available to cement together) will decrease. Also the disruptive viscous forces acting on the newly formed agglomerates will increase. The interplay between the chemistry and the various hydrodynamic effects makes predicting agglomeration behaviour difficult.

In 1997, Mumtaz *et al* [2] proposed a numerical model to determine the shear rate dependence of the agglomeration rate constant. Although the numerical results of this model seem plausible, the model has not been rigourously validated yet.

Several studies have been published that try to couple agglomeration experiments in stirred tank reactors (STRs) to some average shear rate found in such a reactor [3, 4]. This approach is flawed due to the fact that the fluid dynamics of the reactor is oversimplified: it assumes a homogeneous shear rate in the tank. In practice, a large spread in shear rates, as well as in particle concentration, is found in the reactor, making the averaging procedure erroneous [5, 6]. It is the aim of this paper to present a measuring set-up that can properly measure the shear rate dependence of the agglomeration rate constant.

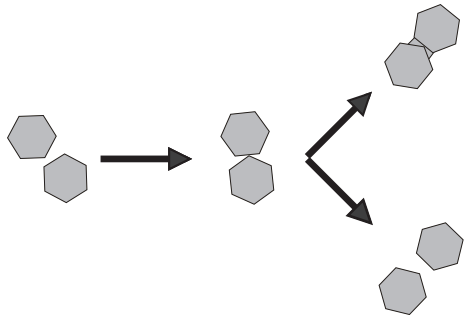

Figure 1. Schematic representation of the agglomeration process.

The technique is based on a cylindrical Couette flow device, in which a near-constant shear field is generated. A super-saturated suspension is introduced in the flow device. The well-defined shear flow will cause the particles to agglomerate. The suspension is illuminated by a pulsed laser. A CCD camera, equipped with a microscope objective and a magnification tube, is used to observe the suspension. By tracking the particle number concentration in time, the agglomeration rate constant at a fixed shear rate can be determined. Repeating the experiment at different shear rates gives the full shear rate dependence of the agglomeration rate constant.

The aim of this paper is to present the experimental technique, including optics, signal processing and the results of various verification experiments. Detailed results on a specific chemical system (calcium oxalate monohydrate) will be reported in a separate paper. In section 2, theoretical considerations for developing the technique are given. In section 3, the construction of the set-up is discussed. Several critical tests are reported to determine the operating window of the experimental set-up, the results of which will be treated in section 4. Finally, section 5 contains concluding remarks.

2. Theoretical background

2.1. Orthokinetic agglomeration

In shear-induced (or orthokinetic) agglomeration, the cause for particle collisions is the velocity difference of the particles induced by velocity gradients in the suspension. In 1917, Von Smoluchowski [1] derived, on the basis of the assumptions that particles are spherical and perfectly follow the fluid, that the particle collision rate in a two-dimensional simple shear flow is given by

$$r_{12} = \beta_{12} N_1 N_2, \qquad \beta_{12} = \frac{\dot{\gamma}}{6}(d_1 + d_2)^3. \tag{1}$$

Under the assumption of mono-dispersity, equation (1) simplifies to

$$r_0 = \tfrac{1}{2}\beta_0 m_0^2, \qquad \beta_0 = \tfrac{4}{3}\dot{\gamma} d^3 \tag{2}$$

where β_0 is the size-independent collision rate constant and m_0 is the particle number concentration, or the zeroth moment of the PSD.

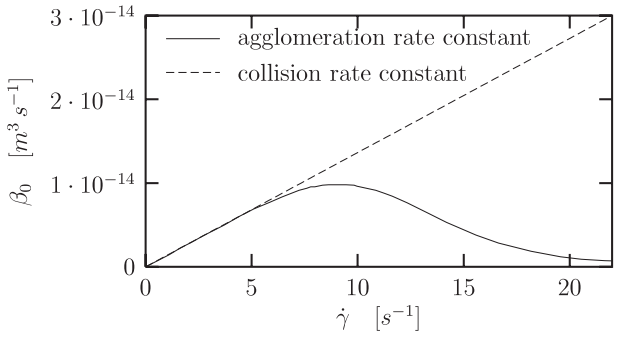

Figure 2. The dependence of β_0 on shear rate, according to Mumtaz *et al* [2]. The curve has been derived for 10 μm $CaOx \cdot H_2O$ particles agglomerating in a suspension at a super-saturation S of 4.7.

In the limit of low shear rates, equation (2) is a good approximation for the agglomeration rate. At higher shear rates, however, the probability that a collision will lead to an agglomeration event decreases due to a relative increase in disruptive forces acting on the agglomerate. This would result in an agglomeration rate constant as a function of shear passing through a maximum and then falling to zero at high shear rates. The first paper to discuss this agglomeration efficiency in detail was from Mumtaz *et al* [2]. They proposed a numerical model in which $\beta_0(\dot{\gamma})$ is determined for a two-dimensional simple shear flow. The collision efficiency was determined by comparing the strength of the chemical bond formed during contact with the viscous forces exerted on the agglomerate. Figure 2 shows this relation for calcium oxalate monohydrate. While the model behaviour is qualitatively correct, experimental validation is still lacking.

2.2. Couette flow device

Up to now, the vast amount of agglomeration research has been performed in STRs. The hydrodynamic conditions found in these reactors make it very difficult to critically evaluate the model by Mumtaz *et al*. Stirred tank flow is inherently transient and three dimensional, and the spread in turbulence levels makes it difficult to define a proper average shear rate as experienced by the particles [5]. Recently, Hounslow *et al* [7] measured β_0 in a laminar Poiseuille flow reactor (PFR). Although the flow in this reactor is much simpler than in STRs, the PFR still exhibits a shear profile. This again results in the need for averaging procedures for interpreting the data, which may bias the results. Two studies mention results of agglomeration experiments in a Couette flow device (see [8, 9]). Unfortunately, both studies present the Couette flow data as part of much more extensive work on agglomeration, in which, for example, reactor type, solution chemistry, etc, are also varied. The choice for operating under unstable flow conditions in both studies, the intrusive measuring techniques used and the lack of information on how the obtained data are interpreted all make the studies less suited for deriving the shear rate dependence of β_0.

In this paper, we present the development of an experimental facility for measuring agglomeration under constant shear conditions, to allow for a rigorous test of the agglomeration model. The set-up consists of a cylindrical

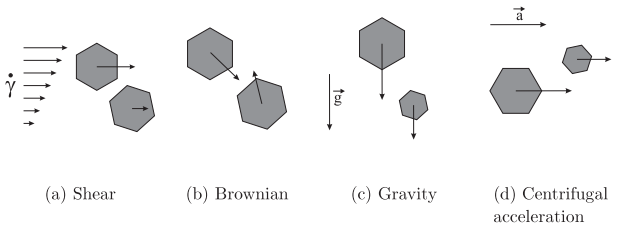

Figure 3. Particle collision mechanisms.

Couette flow device, capable of generating a (nearly) constant shear field and an optical measuring facility that non-intrusively measures particle concentration and size in time. The optical measuring strategy is needed since taking samples from the fluid for off-line analysis would inevitably result in applying shear to the suspension. This would greatly bias the measurements.

While the drastic simplification of the flow field may at first seem to limit the value of this experiment for modelling agglomeration in (industrial scale) agitated tanks, the relevance of this work to industrial type reactors is significant. The particles studied in this work ($d = 10\,\mu$m) are usually smaller than the smallest turbulent length scales typically found in STRs. Assuming a mean turbulent energy dissipation rate of 0.1 W kg^{-1}, common to industrial reactors, the average Kolmogorov length scale is

$$\lambda_k = \left(\frac{\nu^3}{\epsilon}\right)^{1/4} = 56\ \mu\text{m} > d. \tag{3}$$

The particles will therefore experience the viscous flow induced by the smallest scales of turbulence only. This flow is similar to the flow generated in the Couette flow device.

By coupling the local, time-resolved effective shear rate data from numerical simulations of stirred tank flow with the measured agglomeration kernel, a predictive tool for reactor modelling is obtained. In [6], the numerical technique is described for achieving this.

2.3. Particle collision mechanisms

As shown in figure 1, an agglomeration event consists of a collision step (determined by a relative velocity difference between the particles) and an efficiency step (determined by the relative magnitude of the strength of the bond formed between the particles and the disruptive forces acting on the newly formed agglomerate). In this study, we are interested in shear-induced collisions only. Other collision mechanisms may be present, however (figure 3). Note that agglomeration due to shear and Brownian motion acts even if particles are mono-disperse, while a size difference is required for gravity and centrifugal agglomeration.

The relative importance of the collision mechanisms for agglomeration in aqueous systems at room temperature, a density difference between fluid and particles of 1200 kg m^{-3}, a shear rate of 10 s^{-1}, a particle size of 10 μm and a spread in particle size of 5 μm is given in table 1. Since we apply a rotating flow, centrifugal acceleration needs to be taken into account. At a shear rate of 10 s^{-1}, a is 200 times smaller than g (and increases quadratically with shear rate). Centrifugal

Table 1. Relative importance of the various agglomeration mechanisms.

Mechanism		Absolute value	Relative value
Shear	$\beta_{12} = \frac{\dot{\gamma}}{6}(d_1 + d_2)^3$	1.33×10^{-14}	1
Brownian motion	$\beta_{12} = \frac{2}{3}\frac{k_b T}{\eta}\frac{(d_1+d_2)^2}{d_1 d_2}$	1.10×10^{-17}	$<10^{-3}$
Gravity	$\beta_{12} = \frac{\pi g \Delta\rho}{72\eta}(d_1 + d_2)^3\lvert d_1 - d_2\rvert$	2.09×10^{-14}	1.57
Centrifugal acceleration	$\beta_{12} = \frac{\pi a \Delta\rho}{72\eta}(d_1 + d_2)^3\lvert d_1 - d_2\rvert$	1.05×10^{-16}	0.02

acceleration will therefore play a role only at the highest shear rates. It seems that agglomeration due to gravity effects cannot be neglected (it is, in fact, the dominant mechanism). It should be noted, however, that agglomeration rate *constants* are compared here. To compare the overall agglomeration rates, a PSD has to be assumed. The rate constant expressions do show that particles with nearly equal sizes are mostly agglomerating due to shear, while particles with a large size difference will be affected by agglomeration due to gravity. Only with a narrow PSD will particles agglomerate exclusively as a result of shear. Great care has therefore been taken in preparing suspensions with a small spread in particle size. The authors were, however, unsuccessful in fully eliminating collisions due to gravity: obtaining PSDs with a width smaller than 5 μm proved to be infeasible.

Several studies have been published that use laminar Couette flow to determine kinetic relations [10–12]. In these papers, however, collisions in a non-reactive suspension (i.e. aggregation instead of agglomeration) were studied. This allows for the use of well-defined latex particles in a density matched environment, which suppresses the two-phase character of the suspension. For agglomeration research, the chemical reaction taking place in the suspension is crucial. It is therefore not possible to make use of the simplifications mentioned above, due to unwanted changes in the physico-chemistry of the system. The aqueous system can only be density matched by adding large amounts of ionic substances, which would interfere significantly with the solution chemistry of the crystalline material under investigation. Alternatively, the suspension viscosity could be increased by adding water dissolvable polymers. This would limit particle migration due to gravity and centrifugal acceleration, and thus diminish unwanted side-effects. Increasing the liquid viscosity is not an option, however, since polymeric substances are likely to cover the particle surface, which would make interpretation of the data close to impossible. Evidently, the two-phase behaviour (and hence collisions due to gravity) cannot be fully eliminated. This is a complicating factor for interpreting the data.

2.4. Optical measuring system

As mentioned before, orthokinetic agglomeration exhibits a strong coupling with the suspension hydrodynamics. Taking samples from the fluid to monitor the progress of agglomeration is unwanted, since it disturbs the hydrodynamic history experienced by the particles. The optical technique presented here allows for measuring agglomeration non-intrusively. The measuring principle is based on the effect agglomeration has on the particle number concentration of the suspension: in every effective collision, the total number of particles decreases. By tracking the number concentration in time, the agglomeration rate constant can be estimated. The optical set-up, depicted schematically in figure 4, is described below.

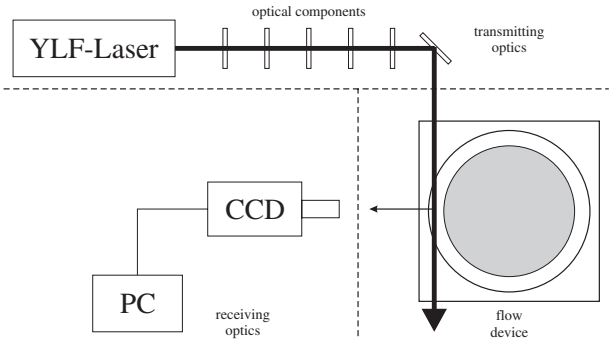

Figure 4. Global representation of the total optical set-up. A sending section, the flow device and the receiving optics can be discerned. The drawing is not to scale.

2.4.1. Receiving optics. In this study, particles with a size of around 10 μm are used. To obtain sufficiently detailed information on the particles, the total resolution of the measuring system aimed for is therefore $\mathcal{O}(1\,\mu\text{m})$. In figure 4, the receiving optics is shown. A CCD camera (512×512 pixels, 250 Hz framerate) is used as a detector. The camera has a resolution of 10 μm/pixel. To obtain the desired pixel resolution, the camera is mounted with an adjustable magnification tube and a long-distance microscope objective (working distance 12 mm, $NA = 0.25$). The receiving optics were set to a magnification of $10\times$, which gives a resolution of 1 μm/pixel. The microscope objective used has a depth of field of approximately 10 μm. While this property makes the alignment of the set-up difficult, it does enable us to work with rather dense particle suspensions. Particles that are out of focus by more than 3–4 particle diameters are already invisible to the system, and will only cause a slight blur in the recorded image. Image analysis will therefore not be hampered by particles out of focus that are in front of the detection volume (figure 6).

The diffraction-limited optical resolution of the system is significantly lower than the pixel resolution. The resolution of a single ideal lens is given by [12]

$$\delta = \frac{0.77\lambda}{NA} \approx 1.5\,\mu\text{m}. \tag{4}$$

The measuring system will have an even lower overall resolution, since the optical errors in the set-up will accumulate. The rotating glass cylinder, discussed below, will especially deteriorate image quality. Furthermore, particles that are out of focus will have an apparent size that is bigger than their real

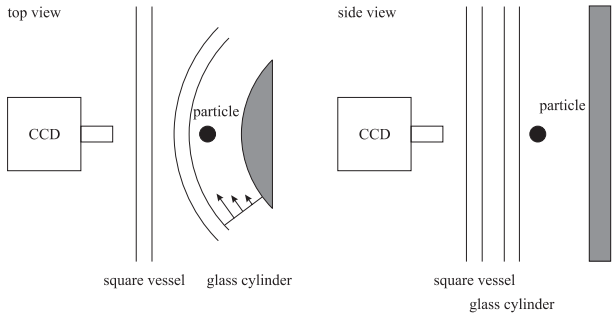

Figure 5. Detailed representation of the flow configuration and receiving optics. Even with the square vessel around the set-up, there is still a slight difference in optical path in horizontal and vertical direction. The errors introduced by this effect are shown to be small.

Table 2. Dimensions of Couette flow device.

	Dimension	Size (mm)	Tolerance (mm)
Glass cylinder	Length	200.0	1.0
Glass cylinder	D_{outer}	106.0	0.04
Glass cylinder	D_{inner}	100.0	0.04
Stator	Length	150.0	1.0
Stator	D_{outer}	90.0	0.01

size. Consequently, PSD information will have a significant bias towards higher particle sizes. The former indicates that acquiring size information from this type of measurement is going to be difficult at best. Obtaining particle number concentrations from the system is feasible, provided that the particle size is much larger than the optical resolution of the system.

2.4.2. Flow configuration. In table 2, the key dimensions of the flow configuration are given. Figure 5 shows that the light reflected by the particles undergoes several optical transitions before reaching the camera. All transitions should be of optical quality to obtain sufficient overall resolution. The rotating glass cylinder in particular should be of lens quality over the entire circumference. The cylinder had a tolerance of 40 μm on both the inside and outside, and was polished to get good optical accessibility. The off-axial oscillation of the cylinder caused by misalignment of the set-up was measured to be around 40 μm also. It should be noted that optical components usually have a tolerance better than the wavelength of the light used (around 0.5 μm) to prevent image distortion. While this 40 μm is still large compared to the wavelength of light, the optical quality appeared to be sufficient for our purposes, as will become evident from experimental results discussed at the end of this paper.

The square vessel around the set-up is incorporated to compensate for the refraction at the glass cylinder. Even in this configuration, the optical path in the horizontal and vertical direction is slightly different. The optical errors introduced this way can be estimated from geometrical optics. A complete description of this calculation is beyond the scope of this paper. Suffice to say that an optical distortion of about 5% between the horizontal and vertical image components is found. This is considered small compared to the errors introduced by the rotating glass cylinder itself and is disregarded in the rest of this work.

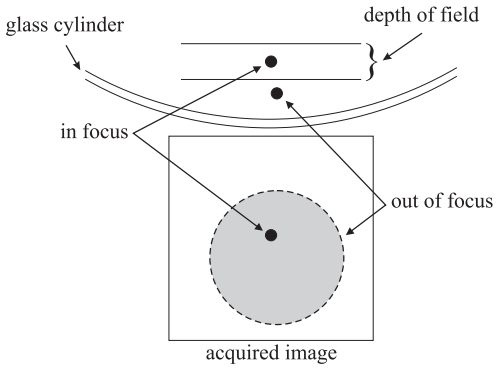

Figure 6. Due to the small depth of field of the receiving optics, particles out of focus will only slightly blur the images. This property makes it possible to work at relatively high particle concentrations.

2.4.3. Sending optics. A difficulty in the optical set-up chosen is that a significant part of the optical path is located in the dense particle suspension. This suspension will scatter a large part of the incident light. To obtain well-exposed images of the suspension, a high intensity light source is required. Also, the exposure time needs to be small to prevent motion blur from occurring. Given the desired resolution of 1 μm, the exposure time should obey the relation:

$$t_{exp} \leqslant \frac{\delta}{v_p} \tag{5}$$

where v_p is a characteristic particle velocity. This velocity is around 0.1 m s^{-1} in our system, which limits the exposure time to 10 μs. These criteria can be met by making use of a pulsed laser as an illumination source. A YLF laser (200 μJ/pulse, <9 ns rise time, repetition rate up to 1000 Hz) is used for this purpose.

Figure 7 shows the sending optics. The laser beam is expanded by a negative and a positive lens (−50 and +400 mm focal length, respectively), a distance equal to the sum of their focal lengths apart. The resulting beam is parallel. A pinhole is placed between these two lenses to remove reflected light from the laser beam. A cylindrical lens ($f = 400$ mm) is used to transform the beam into a sheet. The measuring volume must be illuminated uniformly over the volume height, but the thickness of the laser sheet must be as small as possible, in order to illuminate particles in focus only. The cylindrical lens gave the required degree of freedom to do this. A sheet thickness of about 50 μm was obtained. The final positive lens ($f = 250$ mm) is used to focus the beam at the measuring volume. The mirror is used to guide the beam to the flow device.

It should be noted that, for reasons described in section 2.5.1, it is not possible to distinguish between particles that are in or (slightly) out of focus. This is a serious problem if particle size is measured. Due to the small thickness of the laser sheet, however, the focusing issue is not hampering concentration measurements. In principle, a particle could be located so far from the depth of field of the camera that its image would fill the entire field of view, which would give problems in the image analysis step. The thickness of the laser sheet was chosen such, however, that these particles are not

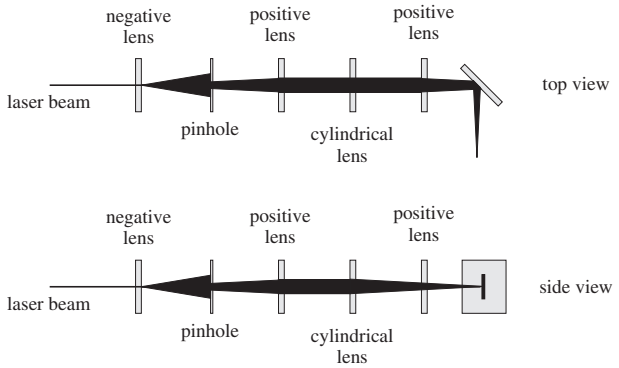

Figure 7. Sending optics to form a vertical laser sheet. The sheet should be very thin in the observation direction. This is to prevent particles outside the depth of field from being illuminated. The sheet should be sufficiently large in the vertical to have a constant illumination over the frame height (5 mm). This is achieved by incorporating a cylindrical lens in the sending optics.

illuminated and are therefore not detected by the camera. In the testing phase of the experimental set-up, it was found that the chance of overlapping blurred particles (which would be erroneously detected as a single particle) was negligible under the above-mentioned illumination conditions.

2.5. Image processing

2.5.1. Speckle pattern due to interference. Once the images are recorded, an off-line image analysis procedure is applied to extract the particle number concentration and the particle size information. Simply converting the raw data to binary images by means of a thresholding operation is insufficient for this purpose. This is due to the use of (coherent) laser light as an illumination source, which causes interference at the particle surface. Due to the surface roughness of the crystals, the light rays scattered by the crystal may have travelled a slightly different optical distance before reaching the camera. A very distinct speckle pattern results. Figure 8 shows an example of this effect.

Figures 8(*b*) and (*c*) show that a plain thresholding operation may seriously bias particle statistics towards higher concentrations, since small high-intensity areas may come loose from the original particle. Simply counting the number of 'white' areas in this binary picture would result in a large number of very small particles, and therefore result in erroneous particle number concentrations. It is therefore essential that the speckle pattern is removed from the images before the thresholding operation is performed. A Gauss filter equation (6) is applied to the images to remove the speckles:

$$G(x_g, s) = \frac{1}{s\sqrt{2\pi}} \exp\left(-\frac{x_g^2}{2s^2}\right). \tag{6}$$

In essence, this filter replaces the original grey value of a pixel by some weighted average of its surrounding. The filter width s is a measure for the spatial frequencies that are removed from the image, and could be chosen such that the speckles vanished.

The typical linear size of the speckles was found to be $\mathcal{O}(3)$ pixels, which was smaller than the observed particle size (10–20 pixels, depending on the mean particle size of the suspension used). By setting $s = 3$ in equation (6), the filter

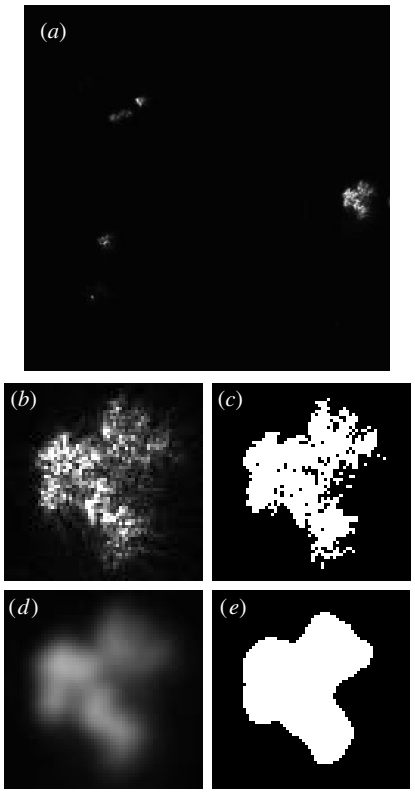

Figure 8. Application of Gauss filter to raw images. The interference pattern is suppressed, which limits the risk of counting spurious amounts of small particles. (*a*) Typical recorded image, image width is 0.5 mm, (*b*) magnification of middle right particle, (*c*) thresholded image, (*d*) Gaussed image, (*e*) threshold of Gaussed image.

could therefore be applied without significantly changing the particle shape. A disadvantange of the filtering operation is the fact that the edge of a particle is altered. As a consequence, the perimeter and the area of a particle can no longer be used to determine average diameters. The image analysis procedure does report a d_{20} based on the particle area after the filtering operation for all the particles that are validated. These data are, however, merely used to investigate trends in the signal and not to obtain quantitative data on particle size. Although the size information is lost, the increase in the reliability of the number concentration measurements justifies the application of the Gauss filter[1].

2.6. Radial particle migration

The rotation of the outer cylinder of the Couette flow device induces a centrifugal force on the particles. Due to their

[1] At the start of this research, it was the intention to reconstruct PSDs with the optical set-up. For that purpose, a criterion had to be defined that could discriminate a particle out of focus from a particle in focus. Particles that are out of focus are observed as blurred particles with a larger size than the real particle size. In principle, the gradient of the grey values provides the necessary information. If a particle is in focus, a large contrast between the particle and the background is observed. The gradient in grey value will therefore be large. Blurred particles will have a more smooth transition from the background to the particle intensity, yielding a lower gradient. It was found, however, that the speckle pattern yielded much higher grey value derivatives than the transition from background to particle. It proved to be impossible to design an algorithm that was able to distinguish between in and out of focus, without altering the particle size and shape. This is why it was decided to focus on measuring the zeroth moment of the distribution, instead of the complete PSD.

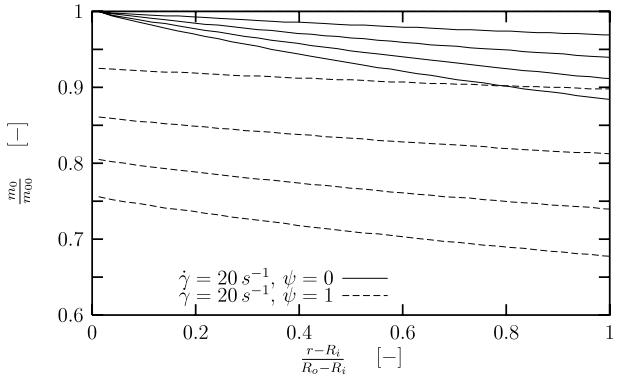

Figure 9. Radial concentration profile in the Couette flow device at 60 s time intervals. If no agglomeration occurs ($\psi = 0$), the particle concentration still decreases in time. This decrease could be mistaken for agglomeration. If all collisions are successful ($\psi = 1$), the radial particle motion would cause an error in the estimated β_0.

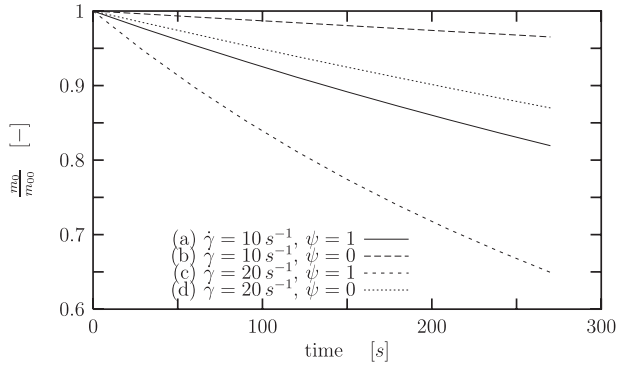

Figure 10. Particle number concentration as a function of time at $r = R_o$ for various conditions. The estimated β_0 from these concentrations without compensating for radial particle migration would be 1.63×10^{-14} (*a*), 2.66×10^{-15} (*b*), 3.93×10^{-14} (*c*), 1.10×10^{-14} (*d*), while the real β_0 was 1.33×10^{-14} (*a*), 0 (*b*), 2.67×10^{-14} (*c*), 0 (*d*), respectively.

small—but non-negligible—inertia, particles will tend to migrate outwards. This effect will cause a particle number decrease in the measuring volume which could be mistaken for agglomeration. This effect can be significant if the real agglomeration rate constant is low (i.e. at the very low and very high shear rates). To account for the centrifugal effect, the total particle number balance is investigated. For a laminar Couette flow with $v_\theta = 0|_{r=R_i}$ and $v_\theta = \omega R_o|_{r=R_o}$, the tangential velocity profile is given by [13]

$$v_\theta(r) = \omega \left(\frac{R_i^2 R_o^2}{R_i^2 - R_o^2} \right) \left(\frac{1}{r} - \frac{r}{R_i^2} \right). \tag{7}$$

The centrifugal acceleration experienced by a particle is given by

$$a = \frac{v_\theta^2}{r} = \omega^2 R_o^4 \frac{(r^2 - R_i^2)^2}{(R_i^2 - R_o^2)^2 r^3}. \tag{8}$$

The radial velocity of a particle can now be derived by assuming a balance between the drag force and the centrifugal force on a particle. Assuming Stokes drag, this relation is given by

$$3\pi\eta d v_{p,r} = \frac{\pi}{6} d^3 \Delta\rho a \quad \Rightarrow \tag{9}$$

$$v_{p,r}(r) = \omega^2 R_o^4 \frac{d^2 \Delta\rho}{18\eta} \frac{R_i^4 - 2R_i^2 r^2 + r^4}{(R_i^2 - R_o^2)^2 r^3}. \tag{10}$$

With equation (10), a balance equation describing the particle number concentration m_0 as a function of radial position and time can be derived:

$$\frac{\partial m_0}{\partial t} = \underbrace{-\frac{1}{r}\frac{\partial}{\partial r}\left(m_0 r v_{p,r}\right)}_{\text{centrifugal displacement}} \underbrace{- \frac{1}{2}\beta_0 m_0^2(r,t)}_{\text{agglomeration}} \tag{11}$$

with the boundary and initial condition:

$$m_0(t = 0) = m_{00}$$

$$m_0(r = R_i) = \frac{1}{\frac{1}{2}\beta_0 t + (1/m_{00})}.$$

Please note that β_0 is taken constant, despite $\dot{\gamma}$ being a weak function of r. The resulting equation provides a framework for estimating the proper agglomeration rate constant from a measured evolution of m_0. The significance of the radial particle migration can be appreciated by some numerical experiments conducted based on equation (11). Figure 9 shows the predicted concentration in the gap between the inner and outer cylinder. Even when agglomeration is turned off (collision efficiency $\psi = 0$), the particle concentration will decrease. This decrease could erroneously be interpreted as agglomeration. Figure 10 shows the time evolution of m_0 close to the outer wall. Estimating β_0 from these data without compensating for radial particle migration would introduce significant errors.

Another complication due to this radial motion is the deposition of a film of particulate matter on the rotating cylinder. As a result, the cylinder becomes less transparent and the signal to noise ratio decreases in time. It might therefore happen that a particle which is visible at the start of the experiment will have an intensity lower than the detection limit at the end of the experiment. This would result in an overestimation of β_0. This effect has been compensated for by introducing a sliding threshold on the particle intensity (figure 11). This concept can best be explained by investigating a typical concentration measurement in detail.

The sliding threshold relies on knowledge about the PDF of the measured intensity. The stochastic nature of the intensity is caused by two effects: light scattering is dependent on particle size and the particles have a size distribution (the influence of the Gaussian intensity profile of the laser sheet is ignored here, since the depth of field of the CCD camera is much smaller than the sheet thickness).

As a first approximation, it was assumed that the scattering intensity is proportional to the surface area of the particle. Figure 12 demonstrates the fairness of this assumption. The quadratic fit in figure 12 has the following form:

$$I = a_1 d^2 + a_2. \tag{12}$$

The offset a_2 is caused by the background noise level of the camera. For this exercise, the PSD is approximated by a Gaussian function (figure 13):

$$\frac{n(d)}{m_0} = \frac{1}{\sigma\sqrt{2\pi}} \exp\left[-\frac{1}{2}\left(\frac{d - \mu}{\sigma} \right)^2 \right]. \tag{13}$$

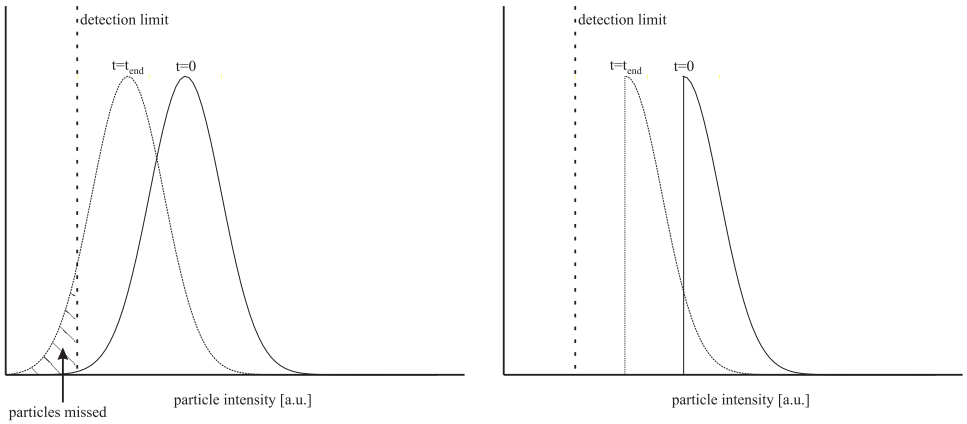

Figure 11. Due to radial particle migration, a film is formed at the outer cylinder during an experiment. This causes the cylinder to become less transparent, which in turn results in lower observed particle intensities. If the particle intensity falls below the detection limit, a significant fraction of the particles could be missed (left). This would result in an underestimation of the particle concentration. To overcome this problem, only particles from the high end of the intensity PDF are counted (right). Provided that the maximum of this PDF is located far from the detection limit, film formation will have little effect on the measured number concentration.

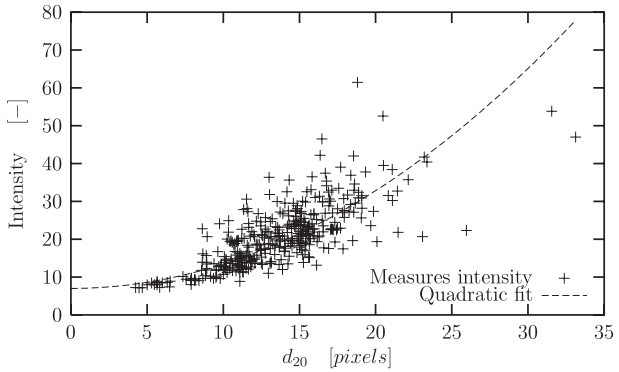

Figure 12. Observed particle intensity as a function of the measured d_{20}. 400 frames acquired in 2 s were used to construct the graph.

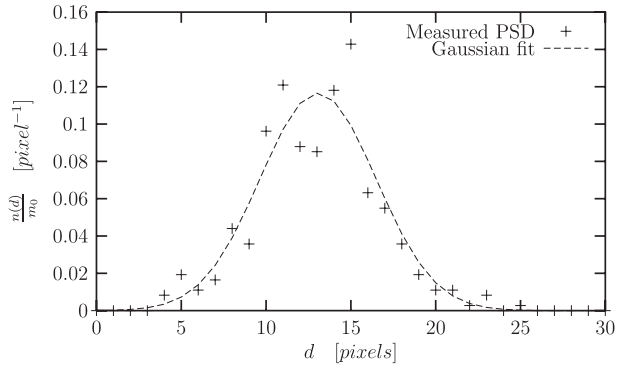

Figure 13. Typical particle size distribution.

Strictly speaking, this distribution is unphysical, since it ranges from $-\infty$ to $+\infty$ (clearly, negative sizes cannot exist). For the PSDs encountered in this work, however, this distribution function fitted the data well. The measured intensity distribution is directly linked to the particle size distribution (equation (12)). Stated differently, the probability that an intensity lower than some value I_b is measured, is given by

$$Pr(I < I_b) = \int_0^{d_p} \frac{n(d)}{m_0} d\,d = \int_0^{d_p} \frac{1}{\sigma\sqrt{2\pi}} \exp\left[-\frac{1}{2}\left(\frac{d-\mu}{\sigma}\right)^2\right] d\,d \tag{14}$$

$$d_p = \sqrt{\frac{I_b - a_2}{a_1}} \quad \Rightarrow \tag{15}$$

$$\Pr(I < I_b) = \frac{1}{2}\left(\operatorname{erf}\left[\frac{1}{2}\sqrt{2}\frac{\sqrt{[(I_b - a_2)/a_1]} - \mu}{\sigma}\right] + \operatorname{erf}\left[\frac{1}{2}\sqrt{2}\frac{\mu}{\sigma}\right]\right). \tag{16}$$

Note that the lower integration limit is taken equal to zero. It is implicitly assumed that equation (13) has fallen to zero for $d = 0$. Differentiating this probability with respect to I_b and dropping the subscript gives the PDF particle intensity:

$$p(I) = \frac{1}{4}\sqrt{\frac{2}{\pi}} \frac{\exp\left[-\frac{1}{2}\left(\frac{\sqrt{[(I-a_2)/a_1]}-\mu}{\sigma}\right)^2\right]}{a_1\sigma\sqrt{[(I-a_2)/a_1]}}. \tag{17}$$

Equation (17) requires four input parameters, being a_1 and a_2 of equation (12) and σ and μ of equation (13). These parameters were fitted to the measured data, as was shown in figures 12 and 13. The analytical result can now be compared to the measured intensity distribution (figure 14). Considering the large scatter in figure 12, we find that the derived intensity PDF represents the measured signal well.

Figure 15 shows that, with decreasing intensity (i.e. decreasing a_1), the intensity PDF changes in shape and shifts towards the lower detection level. Consequently, less particles are detected; the low-end part of the PSD is missed. Ideally, we would like to measure only particles that are not hampered by the detection limit during the entire measurement. As a new criterion for validating a particle, its intensity needs to be equal to or higher than the intensity related to the maximum of the intensity PDF. Provided that this maximum is located far from the detection limit, it will not be hindered by a decrease in intensity. In fact, the integrated area of $p(I)$ from its maximum to infinity

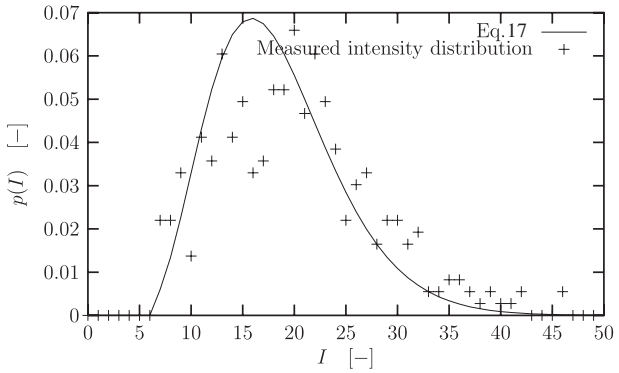

Figure 14. Measured versus derived particle intensity distribution.

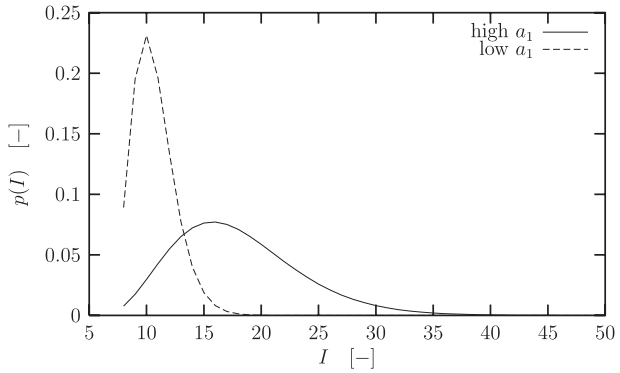

Figure 15. Particle intensity distribution as a function of a_1. The parameter a_1 in equation (12) can be regarded as a measure of the laser intensity. In the case of film deposition on the wall, the effective laser intensity will decrease, which causes the signal to fall closer to the detection limit. The properties of the PSD (i.e. μ and σ) are kept constant in this graph.

($\int_{I_m}^{\infty} p(I)\,\mathrm{d}I$) was found to be independent of a_1 for the parameter range of interest. Since the particle intensity is coupled to the particle concentration (through equations (12) and (13)), the sliding threshold allows for determining a constant fraction of the total number of particles that is unaffected by a decreasing signal to noise ratio. Note that correlating the real number concentration with a constant fraction of the observed particles is as valid as correlating with all the observed particles.

It was found that μ and σ do have a slight effect on $\int_{I_m}^{\infty} p(I)\,\mathrm{d}I$. We tested the variance in this integral in the range $13 \leqslant \mu \leqslant 17$ pixels and $3 \leqslant \sigma \leqslant 7$ pixels (this range covers all the experimental data we have). Changing μ from 13 to 17, while keeping σ constant, resulted in a decrease in area of about 8%. When σ was changed from 3 to 7, the area increased by 26%.

This variation hits upon the weakness in the sliding threshold technique: agglomeration alters the PSD during an experiment, which in turn biases the determination of the particle number concentration. The technique relies on the PSD to remain constant, or at least to vary little, during the experiments. In practice, we are helped by the fact that agglomeration increases both the mean and the variance of the PSD, which causes the errors introduced to partly cancel. Furthermore, our experimental data showed little variation in PSD during an experiment.

It is shown that the sliding threshold technique is not perfect in correcting for the deposition effects. In essence, an assumption is made for the effect of particles missed by the CCD camera, based on particles that were detected. This obviously may result in measuring errors. It is the authors' opinion, however, that this correction procedure is the best technique available.

2.7. Fitting procedure

At this point in the measurement procedure, a set of images has been analysed, which resulted in a set of raw data for the particle number concentration and particle size. After applying the sliding threshold to the concentration data, the corrected data can be used for determining β_0. This is done by subjecting equation (11) to a non-linear regression procedure. Equation (11) was discretized using an explicit finite differencing scheme that is first-order accurate in time and second-order accurate in space:

$$\frac{m_0|_i^{t+1} - m_0|_i^t}{\Delta t} = -\frac{1}{2}(\beta_0 m_0^2)|_i^t - \frac{1}{r|_i}\frac{(m_0 v_r r)|_{i+1}^t - (m_0 v_r r)|_{i-1}^t}{2\Delta r} \tag{18}$$

$$m_0|_{i=1;NR}^{t=0} = m_{00} \tag{19}$$

$$m_0|_{i=0}^{t=0;t_{end}} = \frac{1}{\frac{1}{2}\beta_0 t + 1/m_{00}}. \tag{20}$$

Algorithm 1 gives the structure of the non-linear fitting algorithm. The fitting procedure computes β_0 and m_{00} in camera units. Note that the measuring position (i.e. the radial position at which the measuring volume is located) must be known for this procedure. This position is always located as close to the rotating cylinder wall as possible, to acquire a maximal signal to noise ratio. In the fitting procedure, the location of the measuring volume is therefore assumed to be equal to R_o. Before starting an experiment, the suspensions were always analysed with a Coulter Multisizer II. The real number concentration of the suspension was therefore known. This information is used at the end of the fitting procedure to convert the data from frame units to physical units.

Algorithm 1. Fitting procedure for obtaining β_0 from corrected concentration data.

```
Obtain m00 and d0 from Coulter counter
Retrieve measured concentration data
Make initial guess for β0 and m00 in frame units
while SSres not minimal do
    Integrate eq. (20) based on current β0 and m00
    Compare measured and calculated concentrations
    Generate new estimate for β0 and m00
end while
Convert β0 from frame units to physical units
Report
```

The fitting procedure allows for three levels of complexity of the fitted model. The first level model results from assuming $v_r = 0$, which yields the standard relation for

batch agglomeration. At the second level, accounting for radial particle motion is done by setting $v_r = v_r|_{t=0}$. It is intrinsically assumed that the particles do not change in size during the experiment in this case. At the third level, the measured particle size information is incorporated. Both β_0 and v_r become a function of time in this case. In the fitting procedure, equation (10) is solved for the instantaneous particle size measured. β_0 is mapped back to the initial particle size through

$$\beta_0|^t = \beta_0|^{t=0} \frac{d^3|^t}{d^3|^{t=0}}. \tag{21}$$

This model only gives a very crude description of the size effects occurring during the experiment, and should therefore be used with great care.

If reactive systems are used, super-saturation will be consumed by the particles present, and will thus also be a function of time. While, in principle, this effect should be taken into account, it is the authors' opinion that no adequate model is available that could compensate for this effect. This is due to a combination of the complexity of the solution chemistry and the lack of information on the total crystal surface as a function of time. The measured β_0 for agglomeration will therefore always be a time-averaged quantity.

In spite of the difficulties mentioned, it is worth noting that all models presented are two-parameter models: only β_0 and m_{00} are fitted. One experiment typically consisted of 8000 images, which means that 8000 independent measurements of the particle concentration can be used to estimate two parameters. It is therefore expected that the confidence interval (and hence the uncertainty) for these two parameters will be small.

3. Experimental considerations

3.1. Measuring time

During an agglomeration experiment, an enormous amount of data is being generated. At 200 Hz frame rate, typical data rates of 50 MB s^{-1} are produced. Hard disks cannot cope with such high data rates. The data are therefore buffered in the computer memory, which has a capacity of 1 GB. This would limit us to measuring for 20 s, after which 2–3 min of data saving is needed. Based on a sensitivity analysis of the agglomeration process, we constructed an improved measuring strategy. The sensitivity analysis is described below by considering β_0 in the simplest agglomeration model available:

$$\frac{\partial m_0}{\partial t} = -\frac{1}{2}\beta_0 m_0^2 \quad \Rightarrow \quad m_0(t) = \frac{1}{\frac{1}{2}\beta_0 t + 1/m_{00}}. \tag{22}$$

The sensitivity of the model towards a parameter (here β_0) can be mathematically expressed by

$$\frac{\partial m_0(t)}{\partial \beta_0} = -\frac{\frac{1}{2}t}{\left(\frac{1}{2}\beta_0 t + 1/m_{00}\right)^2}. \tag{23}$$

To find the moment in time at which this sensitivity is maximal, this expression is differentiated with respect to time and set equal to zero. Some algebra gives

$$t_c = \frac{2}{\beta_0 m_{00}}. \tag{24}$$

The time t_c at which the model is most sensitive to β_0 is therefore equal to $2/\beta_0 m_{00}$. Conversely, this is the time at which the measurement gives maximum information on β_0. A similar exercise can be performed on the parameter m_{00} and the radial particle migration can also be accounted for. The analysis then shows that measurements should be concentrated around $t = 0$ (for determining m_{00}) and $t = t_c$ (for determining β_0). By choosing the initial particle concentration, the measuring window can thus be tuned to practical values (i.e. not too small to avoid large influences of experiment start-up and not too long to prevent particle settling effects from coming into play). For our set-up, t_c is chosen around 200 s. A typical measurement now consists of 8 s of image acquisition and 40 s of data saving, which is repeated several times. This way, 8×200 frames containing statistically independent information per time level could be obtained. Note that the parameter β_0 is obviously not known exactly beforehand, but a reasonable estimate can be made from equation (2).

3.2. Suspension preparation

In this research, calcium oxalate monohydrate (COM) crystals are used as a solid phase for the suspensions. The background of this choice is that this material has been studied extensively in the literature. Both growth kinetics and solution chemistry are well documented. It is also known from experiments that this material readily agglomerates, which facilitated the experimental procedure. Finally, the model in figure 2 was derived for this material.

Suspensions are prepared in a glass, baffled stirred reactor, by adding 1 g of COM and 5.85 g of NaCl to 1 l of demineralized water. NaCl is added to raise the ionic strength of the solution, which causes the electric double layer around the crystals to shrink. Under these conditions, the system is in the so-called 'rapid-coagulation regime', which makes interpretation of the data easier (see, e.g., [14]). The PSD of the suspension is now checked. Usually, the mean particle size is far below the desired 10 μm. Particles are grown to the desired size by slowly adding 0.1 M $CaCl_2$ and 0.1 M Na_2Ox solutions. Addition rates of 10–50 ml h^{-1} were used to prevent nucleation and excessive agglomeration from occurring (note that, in this situation, agglomeration is unwanted, since it broadens the PSD of the crystals). The total amount of solution that needs to be added depends on the initial and the desired average particle size. Once the desired mean particle size has been reached, the suspension can be diluted to achieve the desired particle number concentration.

3.3. Typical measurement and processing times

Suspension preparation typically took two days. Agglomeration experiments take 15 min/run and give 2 Gb of data/run. Off-line analysis takes 1.5 s per frame on a standard PIII/500 MHz PC, which means that data could usually be processed overnight.

4. Signal analysis and test results

4.1. Dilution experiments

To check whether or not the response of the system to the particle concentration was linear, a set of dilution experiments

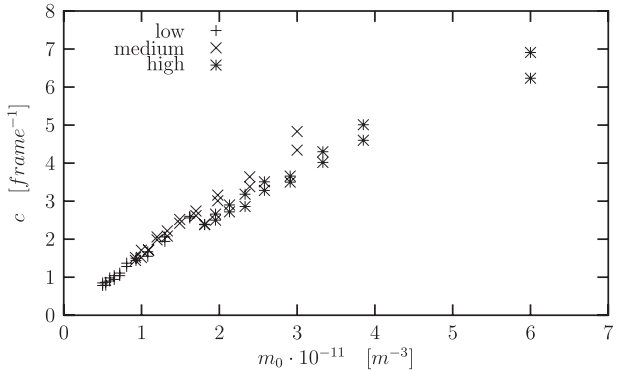

Figure 16. Average number of particles per frame as a function of the particle concentration, obtained from 400 consecutive images. Base concentrations were 6×10^{11}, 3×10^{11} and 1.5×10^{11} m^{-3} for the experiments labelled high, medium and low, respectively.

Table 3. Fit coefficients of the model $y = ax + b$ for the concentration measurements.

Case	$a \times 10^{-11}$ m^3	b
Low	1.57	-4.21×10^{-3}
Medium	1.44	2.07×10^{-1}
High	1.01	6.97×10^{-1}

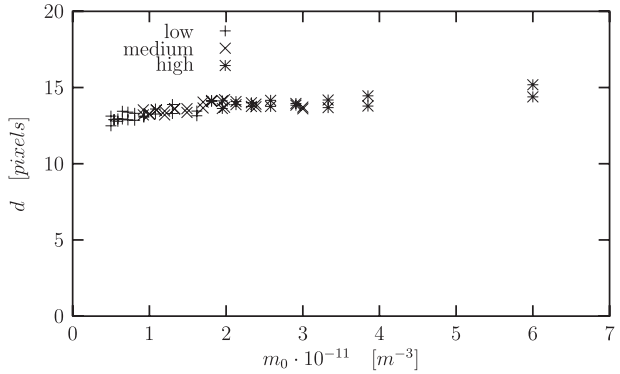

Figure 17. Observed average particle size as a function of particle concentration.

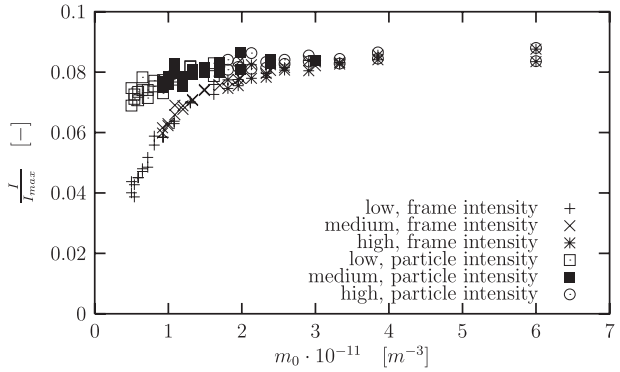

Figure 18. Normalized frame and particle intensity as a function of the particle concentration.

was conducted. A suspension with known concentration and particle size was prepared. The statistics of the suspension were determined with a Coulter Multisizer II, and subsequently measured in the Couette flow device. The suspension was diluted in several steps, which allowed for measurements at a large number of known concentrations. The average number of particles per frame were determined from 400 consecutive frames. Each measurement was taken twice to check reproducibility. The observed particle concentration is expected to be linearly dependent on the preset particle concentration in the low concentration region. The linearity is expected to break down at high particle concentrations. At high suspension density, the images will become poorly illuminated due to extinction, resulting in a poor signal to noise ratio. Also, the chance of a particle being located in another particle's shadow (which could be considered as the equivalent of 'coincidence' in, for example, Coulter counter measurements) will increase. Figure 16 shows the dilution result for particles with a d_{10} of 7.75 μm. For the low and medium concentration measurements, both the linearity and reproducibility appear to be good. The offset from linearity is small in the low concentration case and becomes about 5% for the maximum concentration tested in the medium concentration range (table 3). A slight deflection from linearity can also be witnessed here. In the high concentration case, the measurement seems to be translated by about 10% towards higher concentrations. This was caused by the inaccuracy in the laboratory glasswork used in this measurement. No attempt has been made to correct for this inaccuracy. Clearly, the variance in the measurement increases at these high concentrations. It was therefore decided to conduct measurements at concentrations lower than 2×10^{11} m^{-3}.

To check whether the particles remained constant in size during the dilution experiments, the observed d_{20} based on the projected particle area after filtering out the speckle pattern was plotted against particle concentration (figure 17). No significant trend could be distinguished. The d_{20} was 13.5 ± 0.49 pixels for all measurements. Interestingly, the measured particle size was larger than expected (the mean particle diameter was 7.75 μm; thus an average particle size of about 8 pixels was expected). The main cause for this difference is the Gauss filter in the image analysis step. Recall that the width of the filter used was 3 pixels. Since the filter acts on the entire periphery of the particle, the image could be blurred by 6 pixels over the particle diameter. This indicates that the measured particle size could be around 14 pixels, which is consistent with the observations. It is obvious, however, that there is little hope of obtaining significant size information by this technique. At best, the data can be used for detecting relative changes in particle size within a measurement.

Figure 18 shows the average image intensity, normalized by the saturation intensity of the digital camera. A distinction is to be made between frame intensity and particle intensity. The former refers to an arithmetic mean intensity of all the frames recorded. The latter only considers frames that contain particles. Every frame intensity is normalized by the number of particles it contains. The resulting intensities are averaged and give one 'particle mean' intensity. At low particle concentrations, the number of 'empty' frames (i.e. images containing no particles) will increase. The average frame intensity will therefore decrease. A slight decrease in intensity can also be witnessed when the frame intensity is considered. This indicates that particles are at least partly illuminated

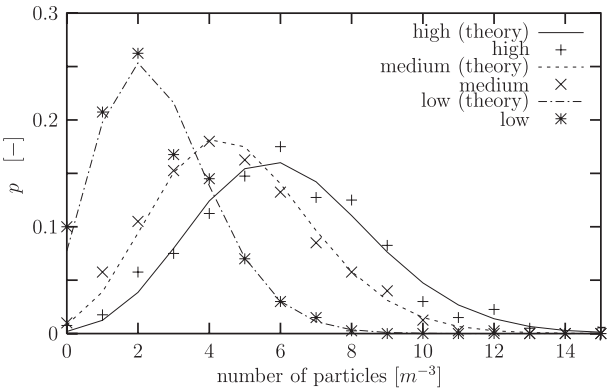

Figure 19. PDF of the number of particles per frame, compared to the theoretical PDF.

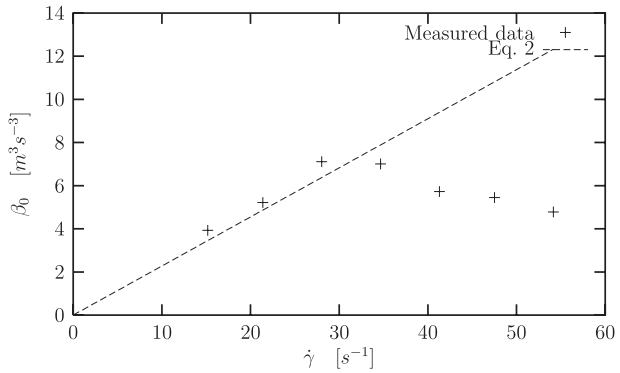

Figure 20. Measured agglomeration rate constants compared to the theoretical prediction of β_0. Although no conclusions can be drawn from only seven experimental points, it seems that the agglomeration rate indeed goes through a maximum at increasing shear rates. These preliminary results give confidence that it is feasible to measure agglomeration rate constants with the experimental facility.

by light scattered from other particles. This secondary illumination will diminish when the particle concentration decreases. Secondary illumination is shown to have a small effect only on the measured particle concentration, as can be seen from the linearity of the concentration response and the measured particle size being constant.

Figure 18 also shows that the average particle intensity is <10% of the maximum intensity that can be handled by the camera. Careful inspection of the data showed that, even under these conditions, some of the pixels were overexposed. Due to the speckle pattern, the average particle intensity is significantly lower than (perhaps 50% of) the maximum particle intensity. Also, since the laser sheet has a Gaussian intensity distribution in the depth direction, it is expected that the average particle intensity will again decrease. To prevent excessive camera noise, it was decided to limit the intensity of the laser light to slightly overexposed particle images, thereby accepting the low average particle intensity and thus a low signal to noise ratio.

4.2. Poisson distribution of the observed number concentration

Since the suspension is well mixed when it is introduced into the Couette flow device, the distance between particles should be randomly distributed. The observed number of particles in a frame should therefore obey Poisson statistics, i.e. the PDF of the number of particles per frame should be described by

$$p(x \text{ particles per frame}) = \frac{\mu^x}{x!}\exp(-\mu) \qquad (25)$$

where μ is the average number of particles per frame. This property was checked for all the measurements taken with the set-up. Figure 19 shows the PDFs at three particle concentrations. As can be seen, the measured distribution is close to the theoretical prediction. This shows that a possible source of error is eliminated by the image analysis procedure: if the above-mentioned speckle pattern was not properly handled, the PDF in figure 19 would be drastically different. The fact that the number of particles in a frame still obeys Poisson statistics gives confidence that the errors introduced by the speckle effect are only minor.

4.3. Time evolution of particle concentration

As a final test, seven agglomeration experiments were conducted. The suspension had an initial particle concentration of 1.5×10^{11} m^{-3}, a mean particle size of 12.0 μm and chemical conditions equal for all experiments. Agglomeration rate constants were determined for $\dot{\gamma}$ equal to 15, 21, 28, 35, 41, 48 and 54 s^{-1}. Six datablocks of 8 s, taken at 1 min intervals, were recorded per experiment, which resulted in $6 \times 8 \times 200$ independent concentration measurements per experiment. The data were analysed with the method described in section 2.7. Radial particle migration was taken into account. The data did not show a significant change of particle diameter in time. Correction for size changes, as described in section 2.7, was therefore unnecessary. The intensity parameter a_1 from equation (12) typically decreased from 0.05 to 0.03 in the course of an experiment. In figure 20, the seven measured points have been plotted together with the theoretical prediction for the collision rate constant (equation (2)).

It is too premature to draw quantitative conclusions from only seven measurements, but it is striking to see the agreement between the expected agglomeration behaviour and the experimental points. For the low shear region, the data are very close to equation (2). The high shear points strongly deviate from this linear relation. The data hint that the agglomeration maximum may be located at higher shear rates than the 10 s^{-1} as predicted by the numerical model by Mumtaz *et al*. This is going to be the subject of further study.

5. Conclusions

An experimental facility for measuring orthokinetic agglomeration has been developed and tested. The method of particle counting by making use of a digital camera and a pulsed laser allowed for non-intrusive determination of agglomeration rate constants. The proposed image analysis scheme was able to correctly determine the particle number concentration in time. After the filtering procedure, the number of particles per image obeyed Poisson statistics, which gives confidence in the measured signal. Drawback of the filtering procedure is that absolute particle size information is lost, and that only relative size information can be extracted from the data.

The measured zeroth moment of the PSD shows a linear response to the suspension concentration for the conditions of interest. Due to radial particle migration and fouling of the Couette flow device, the detection limit (i.e. the minimal particle intensity required for detecting a particle) becomes time dependent. This can be corrected for by introducing a sliding threshold in the image analysis step. This threshold is based on the PDF of the observed particle intensity.

Preliminary agglomeration experiments show that the agglomeration rate constant behaves as is expected from the numerical model predictions by Mumtaz *et al*, although the limited amount of data gathered does not allow for quantitative claims yet. Possible agglomeration effects due to particle size differences (mainly gravity-induced agglomeration) could not fully be eliminated, due to limits on minimum width of the PSD achievable. No method has been found at present that can overcome this flaw. Based on the data gathered so far, this does not appear to be a large problem.

By making use of this technique, rigorous validation of the shear-dependent agglomeration rate constant model proposed by Mumtaz *et al* can be performed. This will be the subject of an future paper by the authors. These data will yield improved insights in agglomeration kinetics, allowing incorporation of detailed agglomeration kinetics in reactor models in the near future.

Acknowledgments

The Particle Technology Group at Delft University of Technology is acknowledged for lending us their YLF laser. The DIOC programme M3 is acknowledged for funding this research.

References

[1] von Smoluchowski M 1917 Versuch einer mathematischen theorie der koagulationskinetik koloider lösungen *Z. Phys. Chem.* **92** 156

[2] Mumtaz H S, Hounslow M J, Seaton N A and Paterson W R 1997 Orthokinetic aggregation during precipitation: a computational model for calcium oxalate monohydrate *Trans. IChemE* **75** 152–9

[3] Collier A P and Hounslow M J 1999 Growth and aggregation rate for calcite and calcium oxalate monohydrate *AIChE J.* **45** 2298–305

[4] van Leeuwen M L J, Huizer C, Bruinsma O S L, Hounslow M J and van Rosmalen G M 1998 The influence of hydrodynamics on agglomeration of aluminum hydroxide: an experimental study *Int. Conf. on Mixing and Crystallization* ed B S Gupta and S Ibrahim (Dordrecht: Kluwer) paper 14

[5] Hollander E D, Derksen J J, Bruinsma O S L, Van den Akker H E A and Van Rosmalen G M 2001 A numerical study on the coupling of hydrodynamics and orthokinetic agglomeration *Chem. Eng. Sci.* **56** 2531–41

[6] Hollander E D, Derksen J J, Portela L M and Van den Akker H E A 2001 A numerical study for orthokinetic agglomeration in stirred vessels *AIChE J.* **47** 2425–40

[7] Mumtaz H S and Hounslow M J 2000 Aggregation during precipitation from solution: an experimental investigation using Poiseuille flow *Chem. Eng. Sci.* **55** 5671

[8] Hartel R W and Randolph A D 1986 *AIChE J.* **32** 1186

[9] Ilievski D, Rudman M and Metcalfe G 2001 The separate roles of shear rate and mixing on gibbsite precipitation *Chem. Eng. Sci.* **56** 2521–30

[10] Calabrese R V, Francis M K, Mishra V P and Phongikaroon S 2000 Measurement and analysis of drop size in a batch rotor–stator mixer *10th European Conf. on Mixing* ed H E A Van den Akker and J J Derksen (Amsterdam: Elsevier) p 149

[11] Serra T and Casamitjana X 1998 Effect of the shear and volume fraction on the agglomeration and breakup of particles *AIChE J.* **44** 1724

[12] Bower C, Washington C and Purewal T S 1995 A combined rheometer and image analyser for characterization of suspensions and aggregates in a shear field *Meas. Sci. Technol.* **6** 196–201

[13] Chandrasekhar S 1961 *Hydrodynamic and Hydromagnetic Stability* (New York: Dover)

[14] Paul C H 1986 *Principles of Colloid and Surface Chemistry* 2nd edn (New York: Marcel Dekker)